Biochemical and Biophysical Research Communications 393 (2010) 426–431

Contents lists available at ScienceDirect

Biochemical and Biophysical Research Communications

journal homepage: www.elsevier.com/locate/ybbrc

Crystal structure of a thermostable Old Yellow Enzyme from *Thermus scotoductus* SA-01

Diederik J. Opperman [a], Bryan T. Sewell [b], Derek Litthauer [a], Mikhail N. Isupov [c], Jennifer A. Littlechild [c], Esta van Heerden [a,*]

[a] Department of Microbial, Biochemical and Food Biotechnology, BioPAD Metagenomics Platform, University of the Free State, Bloemfontein 9300, South Africa
[b] Electron Microscope Unit, University of Cape Town, Rondebosch 7701, South Africa
[c] School of Biosciences, Henry Wellcome Building for Biocatalysis, University of Exeter, Stocker Road, Exeter EX4 4QD, United Kingdom

ARTICLE INFO

Article history:
Received 27 January 2010
Available online 6 February 2010

Keywords:
Old Yellow Enzyme
Flavoprotein
Thermus scotoductus
Thermostability
Enoate reduction

ABSTRACT

Recent characterization of the chromate reductase (CrS) from the thermophile *Thermus scotoductus* SA-01 revealed this enzyme to be related to the Old Yellow Enzyme (OYE) family. Here, we report the structure of a thermostable OYE homolog in its holoform at 2.2 Å as well as its complex with *p*-hydroxybenzaldehyde (pHBA). The enzyme crystallized as octamers with the monomers showing a classical TIM barrel fold which upon dimerization yields the biologically active form of the protein. A sulfate ion is bound above the *si*-side of the non-covalently bound FMN cofactor in the oxidized solved structure but is displaced upon pHBA binding. The active-site architecture is highly conserved as with other members of this enzyme family. The pHBA in the CrS complex is positioned by hydrogen bonding to the two conserved catalytic-site histidines. The most prominent structural difference between CrS and other OYE homologs is the size of the "capping domain". Thermostabilization of the enzyme is achieved in part through increased proline content within loops and turns as well as increased intersubunit interactions through hydrogen bonding and complex salt bridge networks. CrS is able to reduce the C=C bonds of α,β-unsaturated carbonyl compounds with a preference towards cyclic substrates however no activity was observed towards β-substituted substrates. Mutational studies have confirmed the role of Tyr177 as the proposed proton donor although reduction could still occur at a reduced rate when this residue was mutated to phenylalanine.

Introduction

Yeast Old Yellow Enzyme (OYE) was the first flavin containing enzyme isolated [1], but despite extensive characterization of this enzyme, the true physiological oxidant of OYE is unknown. The OYE family of proteins has increased over recent years as homologs from yeast, bacteria and plants have been identified, including morphinone reductase (MR) [2], pentaerythritol tetranitrate (PETN) reductase [3], YqjM [4], xenobiotic (XenA) reductase [5], 12-oxophytodienoate reductase (OPR) [6] and SYE1 [7]. Despite having a conserved overall structure, mechanistic differences and variation in substrate preference occur between the OYE family members [8,9]. Numerous metabolic functions for OYE and its homologs have been suggested, including a role in the oxidative stress response [10,11].

The recent interest in biocatalysis in fine chemical and pharmaceutical sectors, has led to the "rediscovery" and renewed interest in OYE and its homologs [12,13] as it catalyzes the asymmetric reduction of the olefinic bond of α,β-unsaturated carbonyl compounds through trans-hydrogenation [14,15]. Trans-hydrogenation of unsaturated compounds can create up to two new chiral centers [16]. Swiderska and Stewart [17] have illustrated the usefulness of OYE enzymes in stereoselective organic synthesis using the OYE from *Saccharomyces carlsbergensis* where chemo- and stereoselective alkene reductions of a range of α- and β-substituted 2-cyclohexenones were shown to occur with selectivity of up to 96% *ee*. In addition to enoate reduction, members of the OYE family have also been shown to be able to catalyze the reduction of nitro-olefins [18], reductive cleavage of nitro groups from nitroesters including nitroglycerin and pentaerythritol tetranitrate (PETN) and reduction of nitroaromatic compounds including 2,4,6-trinitrotoluene (TNT) [19,20].

Recently, we described a novel chromate reductase (CrS) from the *Thermus scotoductus* SA-01, able to reduce the carcinogen hexavalent chromium to the innocuous trivalent oxidation state through the oxidation of NAD(P)H [11], related to the OYE family. In addition to their intrinsic thermostability, enzymes from thermophilic organisms often also show elevated reaction rates due

* Corresponding author. Fax: +27 51 444 3219.
E-mail address: vheerde.sci@ufs.ac.za (E. van Heerden).

0006-291X/$ - see front matter © 2010 Elsevier Inc. All rights reserved.
doi:10.1016/j.bbrc.2010.02.011

to increased substrate solubility at higher temperatures as well as chemical stability in organic solvents. These properties make them attractive candidates as biocatalysts in industry due to their operational stability.

In this paper, we report the structure of a thermostable OYE homolog in its holoform and its complex with pHBA. The method of proton transfer as part of the enzymatic mechanism has been investigated using site-directed mutagenesis.

Materials and methods

Expression and purification. The complete CrS open reading frame from *T. scotoductus* SA-01 was cloned into the pET28b(+) (Novagen) cloning vector at the *Nde*I and *Eco*RI restriction sites to obtain pET28CrS. Expression was performed in *Escherichia coli* BL21(DE3) cells (Lucigen) at 37 °C and the recombinant protein was purified as a N-terminal histidine tagged protein. Washed cells were resuspended in 20 mM MOPS–NaOH (pH 7.0) buffer and lysed through sonication. The soluble fraction was obtained after ultracentrifugation (100,000*g*, 90 min) of the crude extract. The recombinant CrS was purified using immobilized metal-affinity chromatography (HisTrap FF, GE Healthsciences) and size-exclusion chromatography (Sephacryl S-100HR, Sigma). To obtain full occupancy of the cofactor the CrS sample was incubated with excess FMN before size-exclusion chromatography.

Crystallization. Crystals were grown using the hanging-drop vapor diffusion method at 21 °C. Droplets consisted of equal parts protein (8 mg ml^{-1}) and crystallization (reservoir) solution (0.1 M Tris–HCl, pH 8, and 35% PEG400). CrS in complex with pHBA was obtained by soaking crystals in mother liquor containing 50 mM pHBA for 15 min.

X-ray data collection and structure determination. X-ray diffraction data were collected at the ESRF, BM14 beamline (Grenoble, France) using single crystals and a MarCCD detector. Data were processed and scaled using MOSFLM [21], SCALA and POINTLESS [22]. The CrS structure was solved through molecular replacement using Phaser [23]. Refinement was performed by alternating rounds of model building using the program COOT [24], and crystallographic refinement using Refmac [25] from the CCP4 suite.

Substrate specificity. The reduction of α,β-unsaturated carbonyl substrates was measured through the oxidation of NADPH at 340 or 365 nm. Assays were performed in an anaerobic glove box on a Beckman DU650 UV–vis spectrophotometer. The enzyme was assayed in 1 ml reaction volume containing 20 mM MOPS (pH 6.5), 10 mM $CaCl_2$, 1 mM substrate and 0.1 mM NADPH and varying concentrations of recombinant enzyme at 65 °C.

Mutagenesis. Site-directed mutagenesis of tyrosine 177 to phenylalanine (Y177F) was carried out using the QuikChange mutagenesis method (Stratagene) on the pET28CrS plasmid using the primers 5′-CCA CAT GGC CCA TGG CTT CCT CCT TTC CT-3′ (Y177F forward) and 5′-AGG AAA GGA GGA AGC CAT GGG CCA TGT GG-3′ (Y177F reverse). The mutation was confirmed through sequencing of the gene and expression and purification of the mutant enzyme was performed as described for the wild-type enzyme.

Structural analysis. Hydrogen bonds and salt bridges were evaluated with YASARA-WHATIF [26,27]. A salt bridge was inferred when the side chain carboxyl oxygen atom of Glu or Asp were within 4 Å from the nitrogen atom of Arg, Lys and protonated His side chains. Hydrogen bonds were defined between donor and acceptor heavy atoms with distances less than 3 Å and angles ≥90°. pK_a predictions and accessible surface areas were calculated using YASARA-WHATIF. Graphical presentations were prepared in PyMOL.

Protein Data Bank accession codes. Coordinates and structure factors have been deposited in the Protein Data Bank under the accession numbers PDB ID: 3HF3 and 3HGJ.

Results and discussion

Crystallization of CrS

Characteristic yellow crystals, typically colored due to the oxidized FMN, grew within 3–5 days. Crystals belonged to the space group $P2\ 2\ 2_1$ with unit cell dimensions of a = 101.8 Å, b = 101.9 Å, c = 180.8 Å, $\alpha = \beta = \gamma = 90°$ or the space group $P\ 2$ (a = 98.7 Å, b = 101.2 Å, c = 101.3 Å, $\alpha = \gamma = 90°$, $\beta = 114.3°$). Both lattices have four molecules (monomers) per asymmetric unit (ASU). Upon soaking in pHBA, the CrS crystals changed color to brown and belonged to the space group $P\ 2$ (a = 98.7 Å, b = 101.2 Å, c = 101.3 Å, $\alpha = \gamma = 90°$, $\beta = 114.3°$), also containing four monomers per ASU (Table 1).

The CrS crystals grew as multi-layered sheets that could be readily separated. Thicker sheets having in plane dimensions greater than 1 mm and thickness of 0.2–0.3 mm, which were shown to be large single crystals, were used in the diffraction experiments. The crystal structure showed that the molecules were packed in a lamellar fashion with the layers being formed by octamers having 42 point group symmetry, where the $P2\ 2\ 2_1$ symmetry requires a vertical alignment of every second layer.

Overall structure of CrS

The structure of CrS was solved by molecular replacement using the Old Yellow Enzyme homolog, YqjM as search model and refined at 2.2 Å to an R-factor of 0.174 (Table 1). The CrS structure includes residues 2–349, as the N-terminal region consisting of the histidine tag as well as the N-terminal Met were not defined in the electron density map. The overall core structure of CrS represents the typical eight twisted β-strands surrounded by eight α-helices [$(\alpha/\beta)_8$] or

Table 1
Data collection and refinement statistics.

	Native	pHBA
Data collection		
X-ray source	ESRF, BM14	ESRF, BM14
Wavelength (Å)	0.9537	0.9777
Resolution (Å)	39–2.2 (2.32–2.2)	35–2.0 (2.11–2.0)
Space group	$P\ 2\ 2\ 2_1$	$P\ 1\ 2\ 1$
Unit cell parameters		
$a/b/c$ (Å)	101.8/101.9/180.8	98.7/101.2/101.3
$\alpha/\beta/\gamma$ (°)	90/90/90	90/114.3/90
Unique reflections	90 706 (11 833)	121 277 (17 360)
Completeness (%)	94.7 (85.7)	99.0 (97.0)
R_{merge} (%)[a]	0.130 (0.621)	0.181 (0.564)
Average $I/\sigma(I)$	7.7 (2.6)	8.2 (1.5)
Redundancy	4.6 (4.8)	3.5 (3.2)
Refinement		
R_{work}/R_{free}[b] (%)	0.174/0.214	0.199/0.259
RMSD		
Bond distance (Å)	0.012	0.012
Bond angle (°)	1.36	1.373
Average B-factor (Å^2)		
Protein	22.6	20.3
FMN	14.5	15.0
SO_4	33.6	
Phba		21.5
Solvent	33.4	36.4
Ramachandran distribution (%)[c]	89.8%/10.2%/0%/0%	90.1%/9.8%/0.1%/0%
PDB entry	3HF3	3HGJ

Values for highest resolution shell are indicated in parentheses.

[a] $R_{merge} = \sum_h \sum_J |\langle I_h \rangle - I_J(h)| / \sum_h \sum_J I(h)$, where $I(h)$ is the intensity of reflection h. $\sum_h$ is the sum over all reflections and $\sum_J$ is the sum over J measurements of the reflection.

[b] $R = \sum ||F_o| - |F_c|| / \sum |F_o|$, R_{free} was calculated using 5% of randomly selected reflections that were omitted from structure refinement.

[c] Ramachandran distribution: most favored/additionally allowed/generously allowed/disallowed.

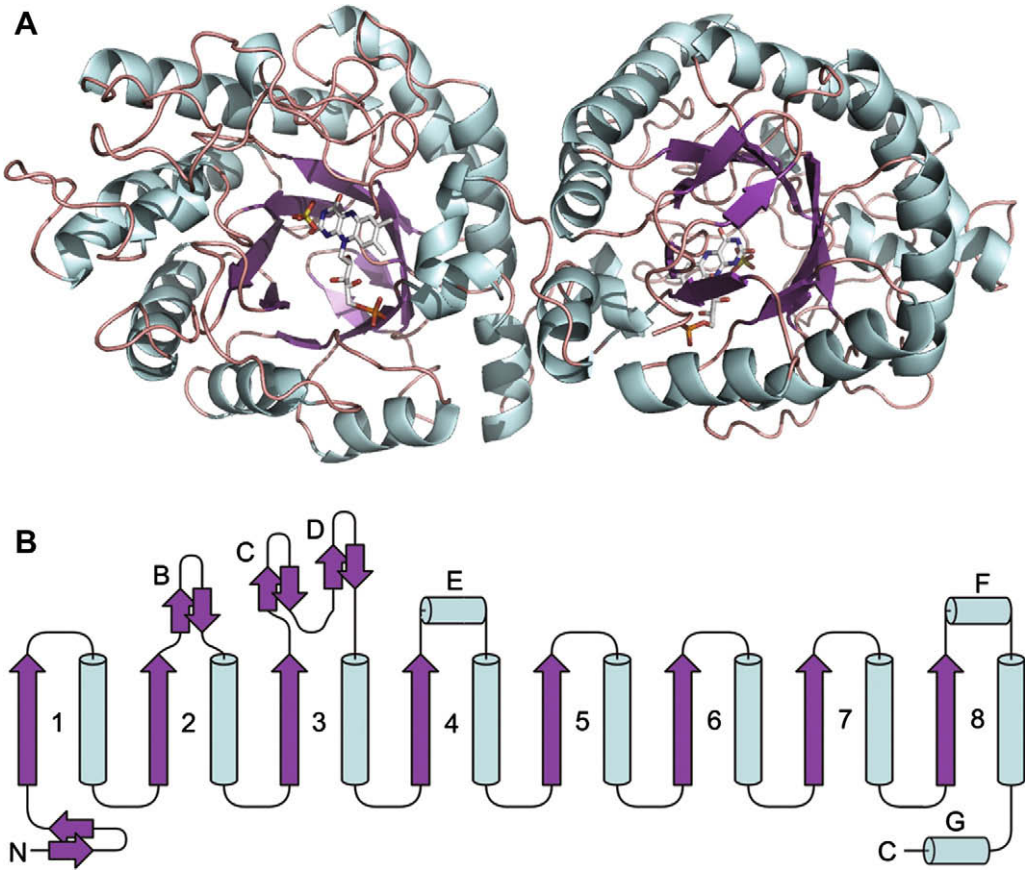

Fig. 1. (A) Ribbon diagram of the *T. scotoductus* CrS dimer. CrS is represented in its oxidized form with the FMN cofactor and bound SO_4 shown as stick models. α-Helices are colored cyan and β-strands purple. (B) Topology diagram of CrS. Helices are drawn as cylinders and β-strands as arrows. Helices and strands forming the core elements are sequentially numbered with the additional secondary structure elements designated by letters. (For interpretation of the references to color in this figure legend; the reader is referred to the web version of this paper.)

TIM barrel structure, (Fig. 1) observed throughout the family of OYE homologs. The closest structural relatives of CrS is XenA and YqjM where 334 residues aligned with a rmsd of 0.9 Å and 337 residues aligned with a rmsd of 1.1 Å, respectively, to CrS.

A β hairpin closes the barrel on the N-terminal side but the C-terminal side is open with an exposed non-covalently bound FMN molecule. Additional secondary structural elements occur on loops formed between the alternating sheet and helix core elements (Fig. 1b) which are the least conserved elements between related structures. The largest loop is formed between β3 and α3 and consists of a parallel and an antiparallel β sheet. This "capping domain" extends towards the C-terminal opening of the barrel.

CrS crystallized as an octamer although the protein exists as functional homodimers in solution [20]. The octamer is formed

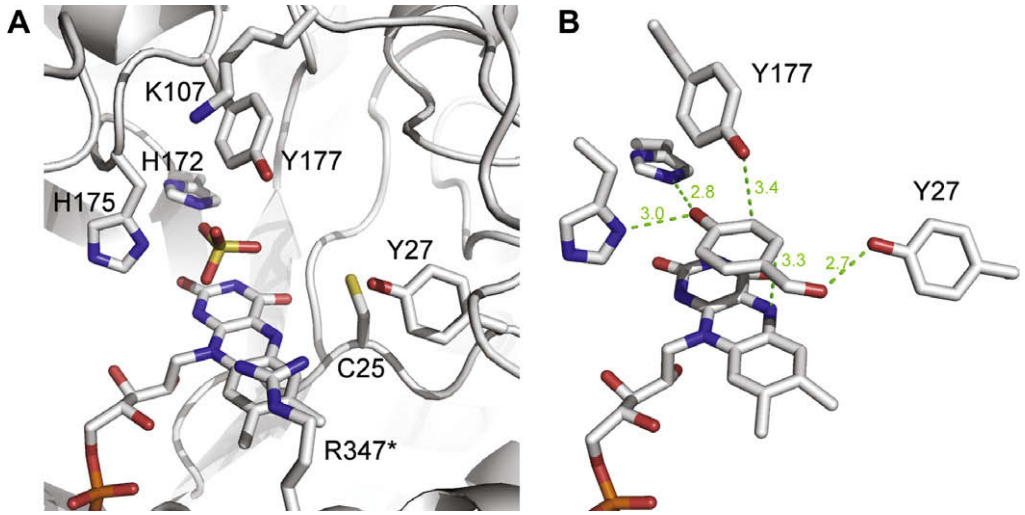

Fig. 2. (A) Active site of oxidized CrS with bound SO_4. Key residues are shown as stick models. Arg347* is from the adjacent monomer. (B) pHBA bound in the active site of CrS.

from dimers by a non-crystallographic fourfold rotational axis and is arranged so that the active sites are all exposed towards the solvent. The monomers making up the biological dimer are related through a twofold crystallographic symmetry axis with the interface contacts involving hydrogen bonding and salt bridges through the interactions of residues from helices α1, α2, α8 and the short helix (F) formed from the loop between α8 and β8. Further monomer interactions occur through the extension of the C-terminal part into the neighboring monomer active site. Upon dimerization, 1230 Å^2 of solvent accessible surface (approximately 9%) is buried per monomer.

Active-site architecture

The FMN cofactor is non-covalently bound in the active site with the *si*-side of the alloxazine ring facing the solvent. The FMN cofactor is bound via extensive hydrogen bonding and hydrophobic interactions with side- as well as main-chain. The substrate binding site is located above the *si*-side of the alloxazine ring of FMN and is occupied by a sulfate ion in the oxidized solved structure (Fig. 2a). Similar to YqjM and XenA, CrS contains a histidine pair (His172 and His175) that corresponds to His191 and Asn194 in OYE, responsible for the positioning and binding of the substrate through hydrogen bonding with the carbonyl oxygen of the substrate. Tyr177, the proposed proton donor, is also conserved and corresponds to Tyr196 in OYE [28]. The ε-amino of Lys107 is within hydrogen bonding distance to Tyr177 and could facilitate the protonation of the substrate by Tyr177 through increasing the general acid properties of the tyrosine. Additional semi-conserved residues include Cys25 (Thr37 in OYE) of which the amide group and sulfydryl groups are within hydrogen bonding distance to N5 and O4 of FMN, respectively, and are proposed to control the redox potential of the FMN cofactor. CrS also resembles YqjM and XenA in that the tyrosine residue involved in certain substrate binding (Tyr27) is located on the N-terminal region as opposed to the C-terminal location in OYE (Tyr375). The major difference between CrS, YqjM and XenA can be found in the length of the "capping domain" between β3 and α3 that extends over part of the active site opening. This domain is much larger than found in YqjM but smaller than the corresponding XenA domain. The extension over the catalytic opening however is similar for CrS and XenA, as the additional loop found in XenA extends outward away from the opening. As with YqjM, an arginine (Arg347) from the adjacent monomer extends into and forms part of the active site.

pHBA was bound by displacement of the sulfate ion (Fig. 2b) and stacked parallel above the isoalloxazine ring of FMN at a distance of 3.2 Å between N5 of FMN and C6 of pHBA. pHBA was bound through hydrogen bonding of the hydroxyl group to His172 and His175 and the aldehyde oxygen to Tyr27. Tyr177 is appropriately positioned at 3.4 Å from the C5 of pHBA for proton transfer to related substrates. Similarly to that of YqjM, the flexible neighboring Arg finger rearranges away from the bound ligand to allow favorable binding.

Structural determinants for thermostability

Comparison of CrS with its closest mesophilic counterparts, YqjM and XenA, shows an increase in proline content (8.1%) for CrS, of which the majority was found within the loops and turns between the alternating core elements. The largest loop (40 amino acids) formed between helices β3 and α3 contains eight proline residues. Due to the pyrrolidine ring structure of proline, the configurational possibilities are restricted not only for the Pro, but also the preceding residue. This decrease in configurational entropy has been shown to aid structural stabilization and contribute to thermostability. Increased proline content is often observed in *Thermus* species due to amino acid bias as a result of their characteristic high GC-content genomes [29].

An increase in intersubunit interactions through hydrogen bonding as well as salt bridges are also observed for CrS. YqjM and XenA are stabilized mostly through simple salt bridges involving single pairs of charged amino acids, whereas CrS favors complex salt bridge networks. The ratio of Arg/Lys residues of CrS (4.6) over YqjM (0.9) and XenA (2.4) indicates a preference towards Arg. Arg has a higher pK_a than Lys and can maintain ion pairs better at higher temperatures than Lys. The three asymmetrical nitrogen atoms also allow three possible directions for interactions, each of which can serve as a proton donor in hydrogen bonding. Three complex salt bridge networks are found at the dimerization interface, of which two of these networks consists of five residues each and the third involving four residues. The complex five-residue salt bridge network between helices α1* and α2 involves Asp37*, Glu85, Arg88, Arg89 and Glu92 (Fig. 3) and shows extensive associated hydrogen bonding.

Reduction of α,β-unsaturated carbonyl compounds

A variety of α,β-unsaturated carbonyl compounds were used for substrate profiling of the OYE homolog's ability to reduce C=C bonds. The OYE homolog shows a broad substrate specificity (Table 2), with 2-cyclohexenone the preferred substrate. CrS exhibits Michaelis–Menten kinetics with 2-cyclohexenone (Fig. 4), with an apparent K_m 3.68 ± 0.24 mM and a V_{max} of 170.7 ± 3.9 μmol min^{-1} mg^{-1}. No

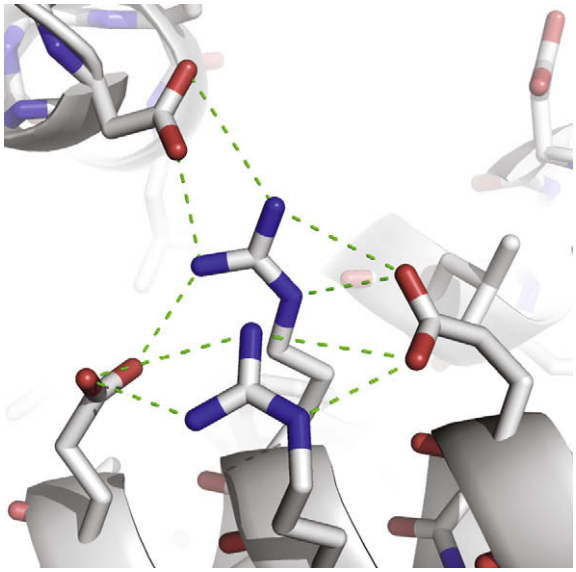

Fig. 3. Ion-pair network between helices α2 and α1* (adjacent monomer) of the *T. scotoductus* CrS dimer.

Table 2
Specific activity of CrS towards α,β-unsaturated carbonyl compounds.

Substrate	Activity ± SD (μmol min^{-1} mg^{-1})
2-Cyclohexenone	27.59 ± 0.47
3-Methyl cyclohexenone	ND[a]
Ketoisophorone	2.56 ± 0.12
Carvone	14.33 ± 0.19
Trans-2-hexen-1-al	3.12 ± 0.27
Trans,trans-2,4-hexadienal	0.15 ± 0.02
Citral	ND[a]
Cinnamaldehyde	1.16 ± 0.07

[a] No activity detected.

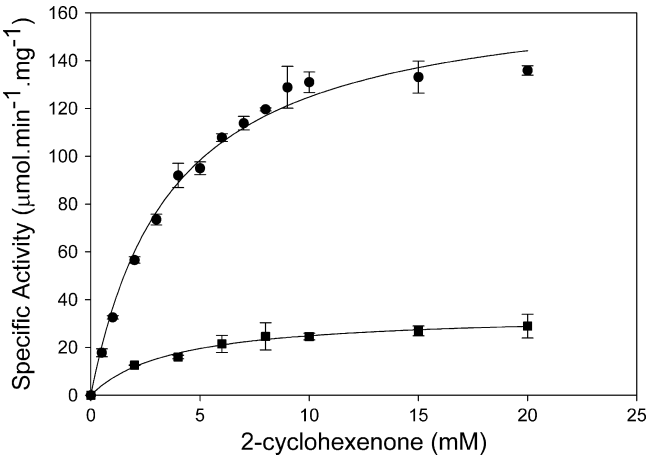

Fig. 4. Steady-state kinetics of purified wild-type CrS (●) and Y177F mutant (■). Error bars indicate standard deviation.

reduction was observed with substrates with substitutions on the β-carbon. A preference was observed towards cyclic substrates.

Reaction mechanism

Based upon the similarity of the catalytic site architecture with OYE and its homologs, we assume an analogous mechanism whereby after the reduction of FMN by NADPH, the substrate is positioned in the catalytic site above the *si* face of the FMN through hydrogen bonding of its carbonyl oxygen to the catalytic-site histidine pair, activating the carbon β for nucleophilic attack through polarization of the C=C bond. This allows the transfer of a hydride from N5 of FMN to the carbon β, with the trans addition of a proton to the carbon α to yield the leaving product. Tyr177 corresponds to the proposed proton donor of OYE (Tyr196), however, in MR this tyrosine residue is replaced by a cysteine (Cys191). Mutagenesis of the cysteine in MR and the corresponding tyrosine (Tyr186) in PETN have shown that despite similar structural architectures, these residues are not key proton donors and that proton transfer is most likely solvent derived [30]. Tyr177 was therefore mutated to phenylalanine (Y177F) to determine whether Tyr177 serves as the proton donor in CrS. The Y177F mutant was still able to reduce 2-cyclohexenone although at a reduced rate. The binding efficiency towards the substrate seems unaffected by the mutation as the apparent K_m was unaltered (Table 3). The catalytic efficiency of Y177F was more than fivefold lower than that of the wild-type enzyme, suggesting Tyr177 does act as a proton donor but in the absence of this catalytic site acid, alternative proton donors might be used. This has been demonstrated by Tu and coworkers [31] for 2,4-dienoyl-CoA reductase (DCR). In the absence of its proposed proton donor (Y166F mutation), DCR still exhibited 27% of the wild-type activity with Glu164 now functioning as the proton donor. Glu164 however did not act as the native proton donor in the wild-type enzyme as confirmed by the different products formed after reduction. In the absence of Tyr177, reduction could possibly continue through alternative proton donation from water as seen for MR as no other active site residues are within credible distance for proton transfer. Alternative binding modes and thus other proton donors are not ruled out as these catalytic mechanisms are postulated mainly from substrate orientations derived from the binding method of artificial ligands such as pHBA. Müller and coworkers [32] related the different product enantiomers of related OYEs to alternative binding modes of the substrate in the active site whereby a "flipped" orientation of the substrate is rotated 180° around the length of the carbon double-bond. Substrate binding orientation is also greatly affected by residues lining the enzyme active site and can result in different stereoselective outcomes for reduction [33].

Table 3
Comparison of kinetic parameters of Old Yellow Enzyme homologs toward 2-cyclohexenone.

Enzyme	K_m (mM)	k_{cat} (s^{-1})	k_{cat}/K_m ($M^{-1}\ s^{-1}$)	Reference
CrS	3.68 ± 0.24	110.1	3.1×10^4	This study
Y177F	3.76 ± 0.85	22.2	5.9×10^3	This study
YqjM	0.293	4.38	1.5×10^4	[10]
XenA	0.033	8	2.4×10^5	[5]
MR	4.2	0.80	1.9×10^2	[2]

Concluding remarks

CrS is an OYE homolog characterized from a thermophile and provides insight into structural stabilization methods for this industrially important class of biocatalysts.

Despite the seemingly overall structural relatedness between the OYE family of enzymes, mechanistic differences are emerging from the growing amount of structural and catalytic data. Their ubiquitous nature but diverse substrate specificities points towards a divergent evolution. The overall eightfold (βα) barrel structure is also among the most frequently observed protein scaffolds within all genomes [34], and their evolution within metabolic pathways has been speculated to have arisen from broad specificity ancestors [35]. Al this makes the OYE family of enzymes an attractive candidate for directed evolution for novel biocatalysts and even designer enzymes.

Acknowledgments

This work was supported by the National Research Foundation South Africa, the Oppenheimer Memorial Trust and BioPAD Metagenomics Platform. The authors thank the BM14 staff at the ESRF, Grenoble, France, for assistance during diffraction data collection.

References

[1] O. Warburg, W. Christian, Über das gelbe ferment und seine wirkungen, Biochem. Z. 266 (1933) 377–411.
[2] T. Barna, H.L. Messiha, C. Petosa, N.C. Bruce, N.S. Scrutton, P.C.E. Moody, Crystal structure of bacterial morphinone reductase and properties of the C191A mutant enzyme, J. Biol. Chem. 277 (2002) 30976–30983.
[3] T.M. Barna, H. Khan, N.C. Bruce, I. Barsukov, N.S. Scrutton, P.C.E. Moody, Crystal structure of pentaerythritol tetranitrate reductase: "Flipped" binding geometries for steroid substrates in different redox states of the enzyme, J. Mol. Biol. 310 (2001) 433–447.
[4] K. Kitzing, T.B. Fitzpatrick, C. Wilken, J. Sawa, G.P. Bourenkov, P. Macheroux, T. Clausen, The 1.3 Å crystal structure of the flavoprotein YqjM reveals a novel class of old yellow enzymes, J. Biol. Chem. 280 (2005) 27904–27913.
[5] J.J. Griese, R.P. Jakob, S. Schwarzinger, H. Dobbek, Xenobiotic reductase A in the degradation of quinoline by *Pseudomonas putida* 86: physiological function, structure and mechanism of 8-hydroxycoumarin reduction, J. Mol. Biol. 361 (2006) 140–152.
[6] C. Breithaupt, J. Strassner, U. Breitinger, R. Huber, P. Macheroux, A. Schaller, T. Clausen, X-ray structure of 12-oxophytodienoate reductase 1 provides structural insights into substrate binding and specificity within the family of OYE, Structure 9 (2001) 419–429.
[7] D. Van den Hemel, A. Brigé, S.N. Savvides, J. van Beeumen, Ligand-induced conformational changes in the capping subdomain of a bacterial old yellow enzyme homologue and conserved sequence fingerprints provide new insights into substrate binding, J. Biol. Chem. 281 (2006) 28152–28161.
[8] A. Brigé, D. van den Hemel, W. Carpentier, L. de Smet, J.J. van Beeumen, Comparative characterization and expression analysis of the four old yellow enzyme homologues from *Shewanella oneidensis* indicate differences in physiological function, Biochem. J. 394 (2006) 335–344.
[9] J.F. Chaparro-Riggers, T.A. Rogers, E. Vazques-Figueroa, K.M. Polizzi, A.S. Bommarius, Comparison of three enoate reductases and their potential use for biotransformations, Adv. Synth. Catal. 349 (2007) 1521–1531.
[10] T.B. Fitzpatrick, N. Amrhein, P. Macheroux, Characterization of YqjM, an old yellow enzyme homolog from *Bacillus subtilis* involved in the oxidative stress response, J. Biol. Chem. 278 (2003) 19891–19897.
[11] D.J. Opperman, L.A. Piater, E. van Heerden, A novel chromate reductase from *Thermus scotoductus* SA-01 related to old yellow enzyme, J. Bacteriol. 190 (2008) 3076–3082.

[12] R.E. Williams, N.C. Bruce, 'New uses for an old enzyme' – the Old Yellow Enzyme family of flavoenzymes, Microbiology 148 (2002) 1607–1614.
[13] R. Stuermer, B. Hauer, M. Hall, K. Faber, Asymmetric bioreduction of activated C=C bonds using enoate reductases from the old yellow enzyme family, Curr. Opin. Chem. Biol. 11 (2007) 203–213.
[14] K. Stott, K. Saito, D.J. Thiele, V. Massey, Old yellow enzyme. The discovery of multiple isozymes and a family of related proteins, J. Biol. Chem. 268 (1993) 6097–6106.
[15] A.D. Vaz, S. Chakraborty, V. Massey, Old yellow enzyme: aromatization of cyclic enones and the mechanism of a novel dismutation reaction, Biochemistry 34 (1995) 4246–4256.
[16] M. Wada, A. Yoshizumi, Y. Noda, M. Kataoka, S. Simizu, H. Takagi, S. Nakamori, Production of doubly chiral compound, (4*R*,6*R*)-4-hydroxy-2,2,6-trimethylcyclohexanone, by two-step enzymatic asymmetric reduction, Appl. Environ. Microbiol. 69 (2003) 933–937.
[17] M.A. Swiderska, J.D. Stewart, Stereoselective enone reductions by *Saccharomyces carlsbergensis* old yellow enzyme, J. Mol. Catal. B Enzym. 42 (2006) 52–54.
[18] Y. Meah, V. Massey, Old yellow enzyme: stepwise reduction of nitro-olefins and catalysis of aci-nitro tautomerization, Proc. Natl. Acad. Sci. USA 97 (2002) 10733–10738.
[19] Y. Meah, B.J. Brown, S. Chakraborty, V. Massey, Old yellow enzyme: reduction of nitrate esters, glycerine trinitrate, and propylene 1,2-dinitrate, Proc. Natl. Acad. Sci. USA 98 (2001) 8560–8565.
[20] R.E. Williams, D.A. Rathbone, N.S. Scrutton, N.C. Bruce, Biotransformation of explosives by the old yellow enzyme family of flavoproteins, Appl. Environ. Microbiol. 70 (2004) 3566–3574.
[21] A.G.W. Leslie, Recent changes to the MOSFLM package for processing film and image plate data, Joint CCP4 + ESF-EAMCB Newslett. Protein Crystallogr. (1992) No. 26.
[22] P. Evans, Scaling and assessment of data quality, Acta Crystallogr. D62 (2006) 72–82.
[23] A.J. McCoy, R.W. Grosse-Kunstleve, P.D. Adams, M.D. Winn, L.C. Storoni, R.J. Read, Phaser crystallographic software, J. Appl. Crystallogr. 40 (2007) 658–674.
[24] P. Emsley, K. Cowtan, Coot: model-building tools for molecular graphics, Acta Crystallogr. D60 (2004) 2126–2132.
[25] G.N. Murshudov, A.A. Vagin, E.J. Dodson, Refinement of macromolecular structures by the maximum-likelihood method, Acta Crystallogr. D53 (1997) 240–255.
[26] E. Krieger, G. Koraimann, G. Vriend, Increasing the precision of comparative models with YASARA NOVA – a self-parameterizing force field, Proteins 47 (2002) 393–402.
[27] G. Vriend, WHAT IF: a molecular modeling and drug design program, J. Mol. Graph. 8 (1990) 52–56.
[28] R.M. Kohli, V. Massey, The oxidative half-reaction of old yellow enzyme. The role of tyrosine 196, J. Biol. Chem. 273 (1998) 32763–32770.
[29] V. Wilquet, M. Van de Casteele, The role of the codon first letter in the relationship between genomic GC content and protein amino acid composition, Res. Microbiol. 150 (1999) 21–32.
[30] H.L. Messiha, N.C. Bruce, B.M. Sattelle, M.J. Sutcliffe, A.W. Munro, N.S. Scrutton, Role of active site residues and solvent in proton transfer and modulation of flavin reduction potential in bacterial morphinone reductase, J. Biol. Chem. 280 (2005) 27103–27110.
[31] X. Tu, P.A. Hubbard, J.A. Kim, H. Schulz, Two distinct proton donors at the active site of *Escherichia coli* 2,4-dienoyl-CoA reductase are responsible for the formation of different products, Biochemistry 47 (2008) 1167–1175.
[32] A. Müller, B. Hauer, B. Rosche, Asymmetric alkene reduction by yeast Old Yellow Enzyme and by a novel *Zymomonas mobilis* reductase, Biotechnol. Bioeng. 98 (2007) 22–29.
[33] S.K. Padhi, D.J. Bougioukou, J.D. Stewart, Site-saturation mutagenesis of tryptophan 116 of *Saccharomyces pastorianus* old yellow enzyme uncovers stereocomplementary variants, J. Am. Chem. Soc. 131 (2009) 3271–3280.
[34] N. Nagano, C.A. Orengo, J.M. Thornton, One fold with many functions: the evolutionary relationships between TIM barrel families based on their sequences, structures and functions, J. Mol. Biol. 321 (2002) 741–765.
[35] R.R. Copley, P. Bork, Homology among $(\beta\alpha)_8$ barrels: implications for the evolution of metabolic pathways, J. Mol. Biol. 303 (2002) 627–640.